BMC Plant Biology

RESEARCH Open Access

Iron-modified biochar modulates root metabolism, mitigates antimony accumulation and enhances growth in rice (*Oryza sativa*)

Renyan Duan[1,2*], Fumin Meng[1], Hui Yang[1], Yihuan Du[1], Qian Dai[1] and Yu Zhang[1]

Abstract

Background Antimony (Sb), with low biodegradability and high bioavailability in plants, poses significant health risks via the food chain due to its chronic toxicity and carcinogenicity. Modified biochar represents a promising amendment for ecological remediation of metal-contaminated croplands, yet the efficacy and mechanisms of its application in mitigating Sb accumulation and improving plant growth in Sb-polluted agricultural systems remain inadequately elucidated and require systematic investigation.

Results In this study, pristine biochar (BC) and iron-modified biochar (FeBC) were prepared from pomelo peel flesh (PPF; *Citrus maxima*), and their effects on rice root growth, Sb content, and metabolism under 30 mg/L Sb stress were evaluated. Treatment with 5 g/L BC and 5 g/L FeBC increased root length by 35.04% and 84.60%, respectively, while reducing Sb accumulation in roots by 25.79% and 28.03%, respectively. Root metabolite analysis showed that, compared to BC, FeBC significantly decreased levels of p-coumaroylagmatine, silibinin, and osmanthuside A by 75%, 37%, and 37%, respectively. Conversely, FeBC elevated levels of (S)-actinidine, phaeophorbide A, and 2-keto-6-acetamidocaproate by 187%, 156%, and 122%, respectively. These altered metabolites were enriched in five key metabolic pathways: phenylalanine, tyrosine, and tryptophan biosynthesis; phenylalanine biosynthesis; lysine degradation; tryptophan metabolism; and pantothenate and CoA biosynthesis. Correlation analysis demonstrated significant interrelationships among biochar-induced metabolites, root growth, and Sb accumulation dynamics under Sb stress.

Conclusions The findings provided the insights that FeBC enhanced rice root metabolism and growth while reducing root Sb accumulation. This study provided a methodological foundation for developing eco-friendly remediation technologies in Sb-contaminated soils to enable safer and more sustainable rice production.

Keywords Antimony, Iron-modified biochar, Pristine biochar, Root growth, Root metabolism

*Correspondence:
Renyan Duan
renyanduan@huhst.edu.cn

Full list of author information is available at the end of the article

Graphical abstract

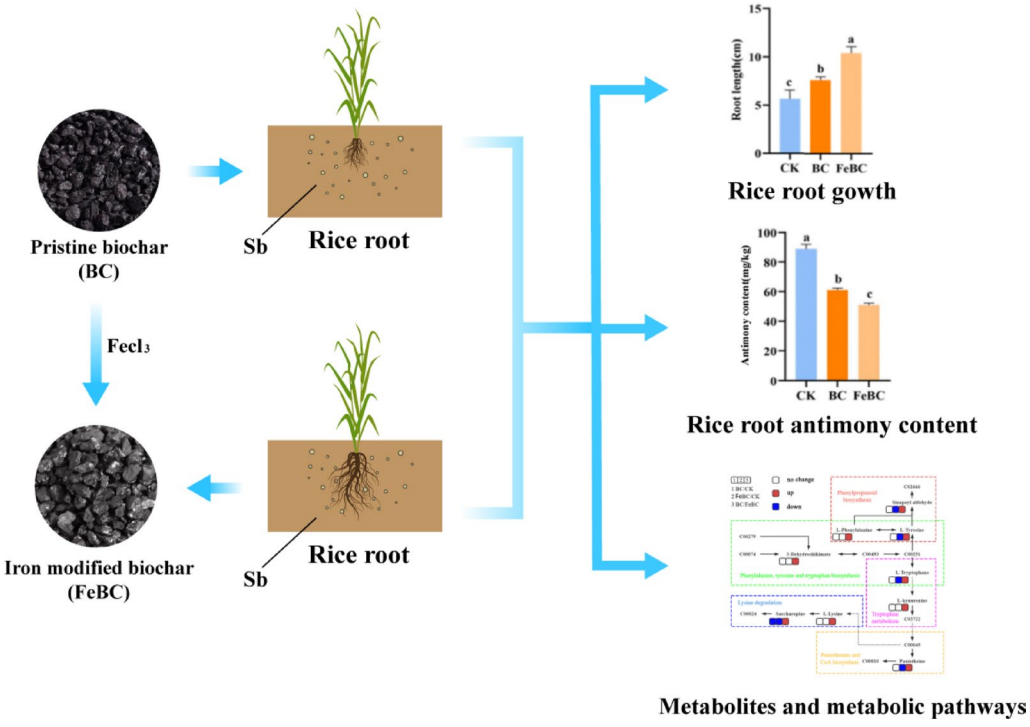

Background

Antimony (Sb), a strategically important heavy metal (HM), is extensively employed in industrial applications including flame retardants, glass manufacturing, and plastic catalysts [1]. Intensive anthropogenic activities such as mining and smelting operations have resulted in widespread Sb contamination of agricultural soils, adversely affecting crop production and threatening both ecosystem stability and public health [2–4]. Epidemiological studies have established associations between chronic Sb exposure and systemic toxicity, including carcinogenic, cardiovascular, immunological, neurological, and reproductive impairments [5]. In plants, Sb stress significantly inhibits growth parameters, reduces biomass accumulation, impairs photosynthetic performance [6], interferes with nutrient uptake [7], and disrupts osmotic balance and hormonal regulation [7, 8]. Due to its environmental persistence and increasing contamination levels, Sb has been designated as a priority pollutant by environmental agencies [9]. The primary route of human Sb exposure occurs through consumption of contaminated crops [10], highlighting the urgent need for effective remediation approaches to reduce Sb bio-availability in agricultural systems and protect human health [11].

Current remediation strategies for heavy metal (HM)-contaminated soils encompass phytoremediation, microbial remediation, and physicochemical approaches [12]. Biochar (BC), a porous carbonaceous material with high chemical stability, demonstrates remarkable potential for HM immobilization in soils while reducing plant uptake [13, 14]. Beyond metal sequestration, BC application improves soil fertility, enhances soil quality parameters, and contributes to carbon storage [13, 14]. Recent research has focused on modified BC variants that exhibit superior stability, specificity, and remediation efficiency compared to pristine BC [15, 16]. Common modification techniques include manganese oxide coating [17], iron modification (FeBC) [18], iron-manganese co-modification [19], and iron-nickel modification [20]. Among these, FeBC demonstrates particularly high HM immobilization capacity and bioavailability reduction while improving soil health indicators [21]. Mechanistic studies reveal that FeBC enhances arsenic-antimony co-contamination remediation through iron-mediated electrostatic attraction and electron complexation, achieving 13.5% and 27.1% reductions in As and Sb bioavailability respectively compared to controls [22]. Similarly, iron-nickel modified rice husk BC exhibits 92.76% toluene removal efficiency, significantly outperforming unmodified BC [20]. These advancements underscore the ongoing optimization of BC modification techniques for enhanced environmental remediation applications.

Research on FeBC for mitigating Sb soil pollution remains limited, with only two studies documented to

date. For example, Teng et al. [23] demonstrated that iron-modified rice husk hydrates reduced lead (Pb) and Sb bioavailability by 25% and 40%, respectively, representing eight-fold and five-fold improvements over unmodified hydrates. Additionally, Tang et al. [24] showed that combining FeBC with *Ochrobactrum oryzae* inoculation enhanced soil nutrient availability, organic carbon content, and enzyme activities, decreasing Sb availability by 46.12% and bioavailability by 59.25%. These studies establish that FeBC primarily immobilizes HMs through synergistic mechanisms including electrostatic adsorption, ion exchange, surface complexation, chelation, co-precipitation, mineral encapsulation, and redox reactions, collectively reducing HM bioavailability and toxicity [23, 25, 26].

Furthermore, root systems dynamically modulate exudate profiles to regulate rhizosphere processes, with emerging evidence highlighting their critical role in HM accumulation. Plants actively restructure their root metabolites to: (1) facilitate nutrient acquisition via chelation and solubilization, (2) immobilize toxic elements through complexation, and (3) enhance biotic stress resistance by secreting antimicrobial compounds [27]. For example, under HM stress, metallophytes such as *Sedum plumbizincicola* elevate alanine exudation, a strategic adaptation that reduces cadmium (Cd) bioavailability while maintaining growth homeostasis [28]. These findings underscore the vital, yet underexplored, link between root exudation patterns and HM phytoavailability.

Pomelo peel fiber (PPF, *Citrus maxima*), an abundant agricultural byproduct, features a hierarchically porous structure with natural honeycomb-like pores in its white flocculent layer. These pores are enriched with hydroxyl and carboxyl functional groups, along with bioactive compounds such as naringin and flavonoids, which collectively provide both physical adsorption sites and chemical binding moieties for HM immobilization [29, 30]. Previous research has established that BC derived from PPF exhibits superior adsorption capacity, rendering it effective for wastewater treatment [31, 32]. However, the potential of PPF-derived BC and its FeBC in alleviating Sb phytotoxicity and accumulation in rice (*Oryza sativa* L.) remains unexplored. We hypothesize that BC and FeBC amendments may mitigate Sb bioaccumulation in rice by modulating metabolic responses under Sb stress. To test this hypothesis, we systematically characterized the structural properties of these biochars and evaluated their effects on root growth and metabolic profiles using metabolomic approaches. This study can provide novel insights into the mechanisms underlying Sb immobilization and metabolic reprogramming in rice, offering valuable guidance for developing phytoremediation strategies in Sb-contaminated paddy systems and optimizing functionalized biochar materials.

Materials and methods

Biochar materials

Fresh PPF samples were sectioned into 2 cm^3 cubes and dehydrated at 100 °C in a convection oven. The dried material underwent pyrolysis in a muffle furnace (500 °C, 2.5 h) under oxygen-limited conditions [33]. The resulting biochar was cooled to 70 °C under ambient conditions prior to characterization. For FeBC synthesis, we employed a hydrothermal modification protocol [34]. Briefly, $FeCl_3$ was dissolved in ethylene glycol and sonicated (30 min). After cooling, biochar and ammonium acetate were introduced under continuous stirring. The mixture was transferred to a 100 mL high-pressure reactor (20 bar rating) and heated (200 °C, 12 h). The product was subsequently treated with 50% (*v/v*) HNO_3 (5 h stirring) to enhance surface hydrophilicity and iron oxide formation. The modified material underwent rigorous washing (> 3 cycles) with deionized water under dynamic agitation until achieving neutral pH (7.0 ± 0.2), verified by real-time monitoring. Between cycles, samples were equilibrated (10 min) to minimize measurement artifacts from residual acidity. Final products were oven-dried (60 °C) and stored for subsequent analyses [35].

Determination of BC properties

Surface morphology of BC and FeBC samples was analyzed using scanning electron microscopy (SEM). Samples were dispersed in anhydrous ethanol via sonication, then deposited onto conductive adhesive-mounted aluminum foil. After infrared drying, specimens were gold-coated prior to SEM imaging [36].

Crystalline structure and phase composition were determined by X-ray diffraction (XRD) analysis [37]. Scans were performed from 10° to 80° (2θ) at 2°/min with 0.04° sampling intervals. Mineral identification was achieved through d-spacing analysis of characteristic diffraction patterns [38].

Elemental composition analysis was performed using energy dispersive spectroscopy (EDS) coupled with scanning electron microscopy. Samples (30 mg) were pretreated through milling and drying procedures before being mounted on conductive adhesive tape. EDS analysis was conducted by collecting characteristic X-rays emitted from electron beam-excited FeBC samples, enabling simultaneous elemental mapping and quantitative analysis [39]. Acquired X-ray spectra were processed to determine both qualitative and quantitative elemental distributions [40].

Functional group characterization was performed using a Thermo Nicolet iS5 FTIR spectrometer [41]. Prior to analysis, 30 mg aliquots of BC and FeBC samples

were thoroughly dried to minimize spectral interference from moisture. Samples were homogenized with KBr (1:100 ratio) and ground to < 2 μm particle size. FTIR spectra were acquired in the 400–4000 cm^{-1} range with 5 mm optical path length [42]. All spectra underwent standard preprocessing including baseline correction and noise reduction prior to comparative analysis of functional group signatures.

Plant culture

Rice cultivation was conducted hydroponically using modified Hoagland solution. Seeds of *O. sativa* were surface-sterilized with 8% (*v/v*) H_2O_2 for 20 min, followed by deionized water rinsing. Germination was carried out in distilled water at 25 ± 1 °C under dark conditions for 10 days. Uniform seedlings were then transferred to hydroponic systems (85 × 85 × 5 cm) containing quarter-strength Hoagland solution for 3 days acclimation, with subsequent nutrient concentration adjustment to half-strength for seven days [6, 43].

Seedlings (1 cm root length) were transferred to 50% Hoagland solution containing 30 mg/L Sb ($C_8H_4K_2O_{12}Sb_2 \cdot 3H_2O$) [44]. This Sb concentration reflects environmental contamination levels, with reported values ranging from 37 to 63 mg/L in polluted rivers to 1,300 – 21,790 mg/L in mining wastewater [45]. Previous studies have used 10–50 mg/L of Sb to examine its phytotoxic effects on rice [46]. Three experimental groups were established: control (Sb only), Sb + pristine BC (5 g/L), and Sb + FeBC (5 g/L). The biochar dosage was selected based on previous hydroponic studies demonstrating effective contaminant mitigation at 1.3–26.6 g/L [47] and optimal plant growth enhancement at 5 g/L [48].

Each treatment comprised three replicates with 12 plants per replicate (36 plants total). Sb(III) solution was renewed every three days by replacing 50% of the volume [49]. Plants were maintained at 25–30 °C, 51–63% relative humidity, and 12 h natural photoperiod. After 4 weeks, roots were analyzed using an LA-S system for length measurement. Roots were then divided into two subgroups: one for Sb quantification and another for metabolite profiling [41, 50].

Determination of Sb content

Root samples (0.2 g) were digested in 100 mL tubes with 10 mL mixed acid (perchloric acid and nitric acid in a ratio of 3:10) at room temperature for 12 h. Digestion was completed using an HM digester at 135–145 °C. The digestate was transferred to 25 mL volumetric flasks, diluted with 1% HNO_3, and homogenized prior to analysis [51]. Sb concentrations were quantified by atomic absorption spectrometry (pinAAcle 900) [52].

Measurement of root metabolism

Root samples from CK, BC, and FeBC treatments were rinsed with phosphate-buffered saline (pH 7.0) and flash-frozen in liquid nitrogen (15 min). Metabolites were extracted with 0.8 mL 100% methanol and 10 μL phenylalanine, followed by sequential homogenization (60 Hz, 3 min), ice-water bath sonication (40 kHz, 30 min), and centrifugation (12,000 rpm, 15 min, 4 °C). Filtered supernatants (0.22 μm) were analyzed by LC-MS (QE mass spectrometer) in both ESI+ (3.5 kV) and ESI- (–2.5 kV) modes with the following parameters: gas flow 11 L/min, temperature 350 °C, mass range m/z 81-1000 (resolution 60,000). Mass axis accuracy was dynamically monitored throughout analyses [53].

Statistical analysis

Root length, Sb content, and metabolomic data were analyzed using SPSS 23.0 and GraphPad Prism 8.0.1. Significant differences among treatment groups were determined by one-way ANOVA with Tukey's post hoc test ($p < 0.05$) [41].

Results

Comparative analysis of BC and FeBC characterization

There were notable differences in the surface structure between BC and FeBC (Fig. 1). The surface of BC was smooth (Fig. 1a), with striated cracks and pores of different diameters (Fig. 1c and e). FeBC formed a new surface structure, with a rough surface and some small particles visible (Fig. 1b) as well as obvious honeycomb and tubular porous structures (Fig. 1d and f). EDS confirmed that the atomic percentages of C, O, and Fe in FeBC were 75.5%, 19.6%, and 4.9%, respectively (Fig. 2A). EDS found that Fe was evenly distributed on the surface of the FeBC (Fig. 2B and C).

Infrared spectroscopy analysis confirmed that the structures of FeBC and BC both ha*d* an absorption peak at 3433 cm^{-1}, which was the vibration of C-C bonds, indicating that the structures of both FeBC and BC were stable (Fig. 3A and B). XRD analysis confirmed that diffraction peaks appeared at 2θ angles of 18.28°, 30.07°, 35.42°, 37.05°, 43.04°, 47.13°, 53.34°, and 62.50°. After matching and comparing with X-ray standard cards (89–0950), it was determined that the product was iron tetroxide (Fe_3O_4) with good crystallinity (Fig. 3C).

Significant alterations in root length and Sb concentration induced by BC/FeBC treatments under Sb stress

In the 0 mg/L Sb treatment group, neither the addition of BC nor FeBC resulted in a significant effect on root growth ($p > 0.05$) (Fig. 4A). In the 30 mg/L Sb treatment group, the addition of both BC and FeBC significantly improved root growth. Compared to the CK, the BC group increased root length by 35.04% ($p = 0.0012$) and

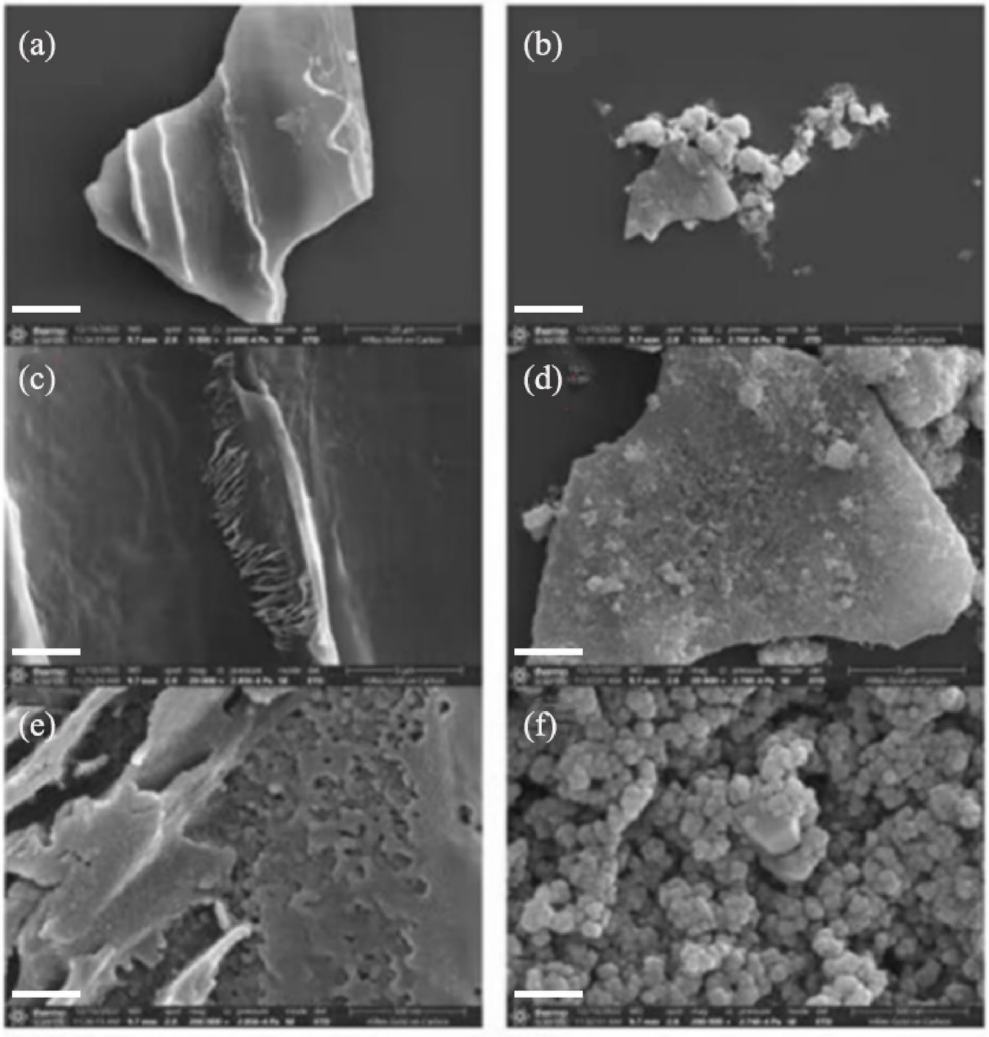

Fig. 1 Scanning electron microscopy images showing morphological differences between BC (**a**, **c**, **e**) and FeBC (**b**, **d**, **f**). Scale bars were 20 μm (**a**, **b**), 5 μm (**c**, **d**), and 500 nm (**e**, **f**), respectively

the FeBC group increased root length by 84.6% ($p < 0.001$) (Fig. 4B). In the 30 mg/L Sb treatment group, the addition of BC and FeBC significantly decreased the Sb concentration in the roots. Compared to the CK group, the BC group and the FeBC group reduced Sb concentration ($p < 0.001$) by 25.8% and 28.03%, respectively ($p < 0.001$) (Fig. 4C).

Metabolic alterations in rice roots induced by BC/FeBC treatments under Sb stress

The PLS-DA results demonstrated the complete separation of metabolites in the anionic and cationic modes in the CK, BC, and FeBC groups. This indicated that the BC and FeBC treatment significantly altered the metabolite profiles of rice roots (Fig. 5A and B). The PLS-DA model showed that R2 was above Q2 in both cation and anion modes, and the intercepts of the Q2 regression line and the Y-axis were −0.0005 and 0.3403, respectively. This indicated that the model fit well with strong predictability, and was suitable for subsequent data analysis (Fig. 5C and D).

Compared to the CK, there were 242 and 483 different metabolites in the BC and FeBC treatments, respectively (Fig. 6A and B), and 349 different metabolites between the BC and FeBC treatments (Fig. 6C). The top 30 metabolites with the most significant differences between different treatments included six glycosides, six organic acids, four lipids, and 14 other compounds (Table 1).

Compared to the CK, the FeBC group significantly decreased the relative abundance of isowertin 2”-rhamnoside ($p = 0.3614*10^{-4}$), cyanidin 3-O-(6”-malonyl-3”-glucosyl-glucoside) ($p = 3.784e-7$), and 2-hydroxybenzaldehyde O-[xylosyl-(1->6)-glucoside] ($p = 0.2591*10^{-4}$), protocatechuic acid 4-glucoside

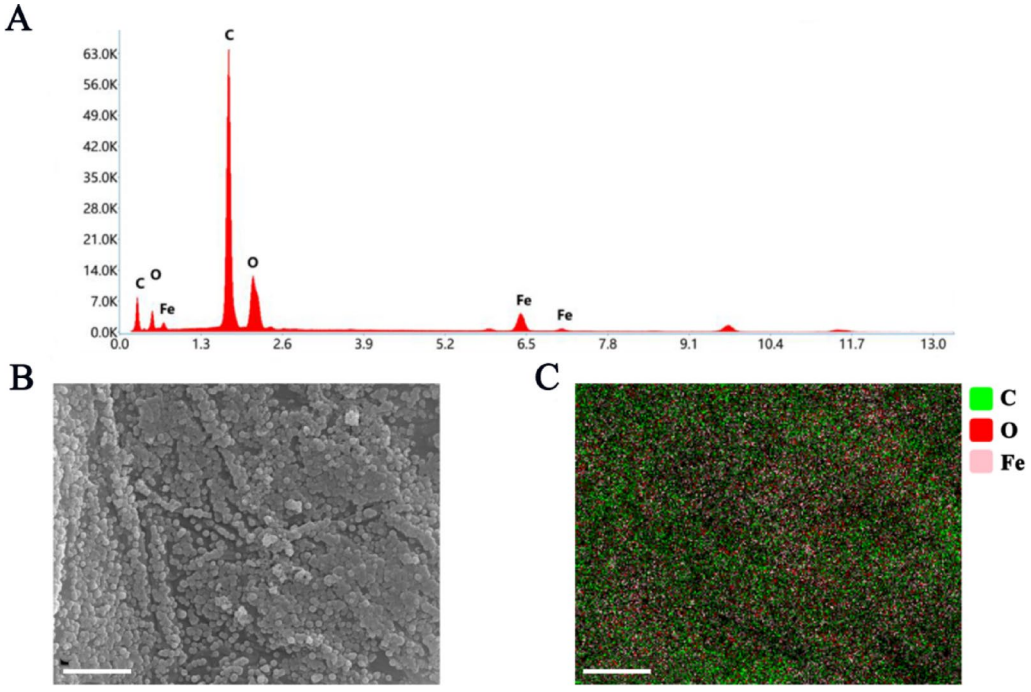

Fig. 2 Elemental composition analysis of FeBC by EDS. **A** EDS image of FeBC; **B** an electron microscope image of FeBC; **C** the elemental distribution of magnetic biochar. Scale bars in **B** and **C** were both 5 μm

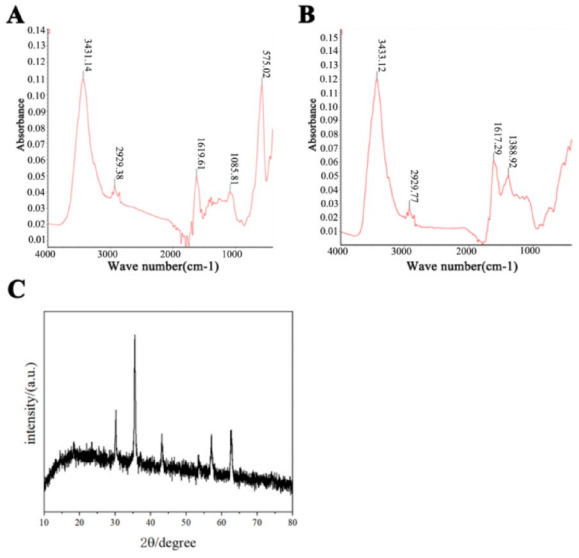

Fig. 3 Spectroscopic analysis showing **A** BC and **B** FeBC by FTIR, with **C** crystalline structure of FeBC by XRD

($p = 3.387e\text{-}7$), swertiamarin ($p = 0.1851*10^{-5}$), by 39%, 30%, 14%, 24%, and 28%, respectively. Compared to the CK, the FeBC group significantly increased the relative abundance of 2-keto-6-acetamidocaproate ($p = 0.206*10^{-4}$), (S)-actinidine ($p = 0.3878*10^{-5}$), and 4-methylimidazole ($p = 0.7318*10^{-4}$), by 124%, 186%, and 138%, respectively (Table 1).

Compared to the BC, the FeBC group significantly decreased the relative abundance of lepidimoic acid ($p = 0.01051$), p-coumaroylagmatine ($p = 0.2724*10^{-5}$), osmanthuside A ($p = 0.4873*10^{-4}$), silibinin ($p = 0.2335*10^{-4}$), and sojagol ($p = 0.7082*10^{-3}$), by 23%, 75%, 37%, 37%, and 35%, respectively. Compared to the BC, the FeBC group significantly increased the relative abundance of indole-3-acetaldehyde ($p = 0.366*10^{-2}$), 2-keto-6-acetamidocaproate ($p = 0.1729*10^{-4}$), (S)-Actinidine ($p = 0.4273*10^{-5}$), and phaeophorbide a ($p = 0.1353*10^{-5}$), 4-Methylimidazole ($p = 0.7057*10^{-4}$), by 111%, 122%, 187%, 156%, and 109%, respectively (Table 1).

BC remediation had a significant impact on the metabolism of rice under Sb stress (Fig. 7). The main metabolic changes between the CK group and the BC group were enriched in (1) biosynthesis of starch and sucrose metabolism, (2) pantothenate and CoA biosynthesis, (3) phenylpropanoid biosynthesis, and (4) biotin metabolism (Fig. 7A). The main metabolic changes between the CK group and the FeBC group were enriched in (1) tryptophan metabolism, (2) lysine biosynthesis, (3) phenylpropanoid biosynthesis, as well as (4) tropane, piperidine and pyridine metabolism (Fig. 7B). Between the BC group and the FeBC group, the main metabolic changes were enriched in (1) tryptophan metabolism, (2) pantothenate and CoA biosynthesis, as well as (3) phenylalanine, tyrosine and tryptophan biosynthesis (Fig. 7C). In total, the BC group and the FeBC group mainly affected plant metabolism through the following five metabolic pathways: (1) phenylalanine, tyrosine, and tryptophan biosynthesis, (2)

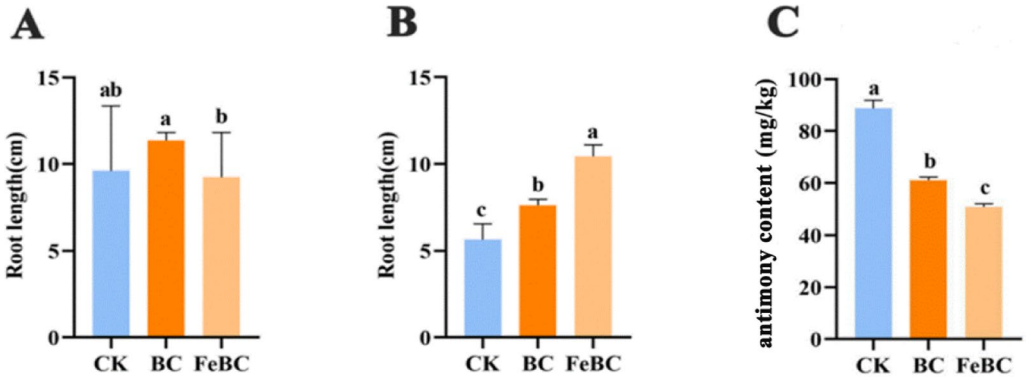

Fig. 4 Impact of biochar and iron-modified biochar on rice root growth and antimony accumulation. The length of rice in 0 mg/L (**A**) and 30 mg/LSb exposure (**B**). Sb contents of the rice root in 30 mg/L Sb exposure (**C**)

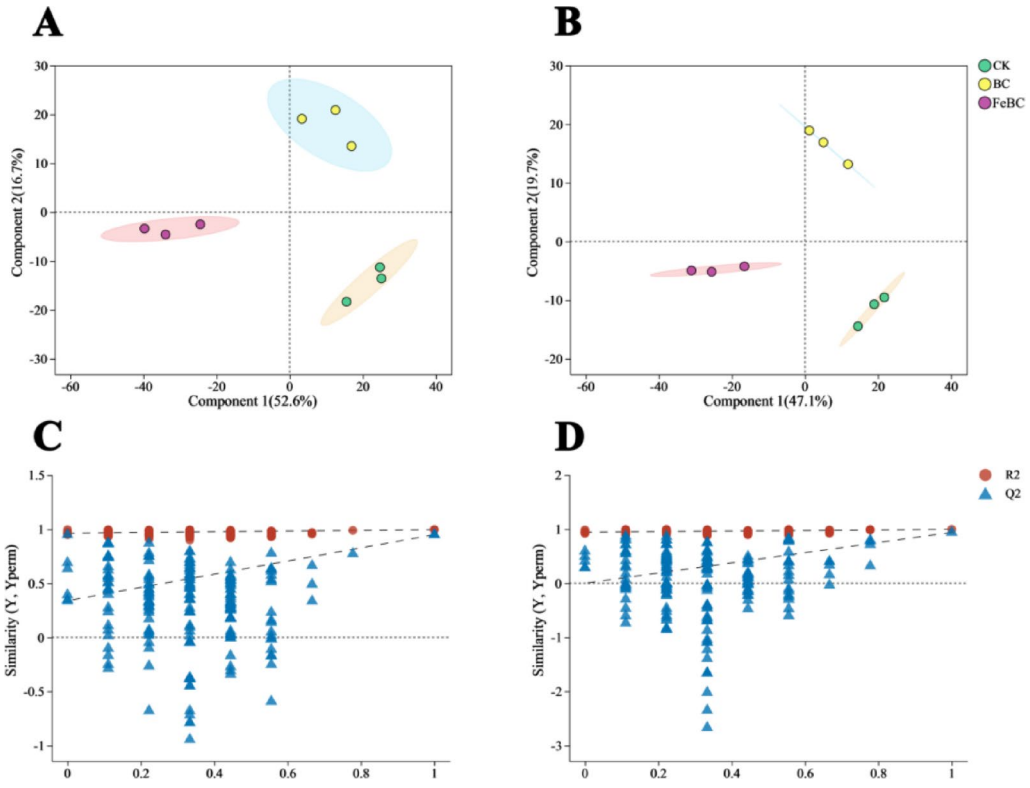

Fig. 5 Partial least squares discriminant analysis (PLS-DA) score plots (**A** and **B**) and corresponding validation plots for BC and FeBC in both positive (NT-pos) (**C**) and negative (NT-neg) (**D**) ionization modes

phenylpropanoid biosynthesis, (3) lysine degradation, (4) tryptophan metabolism, and (5) pantothenate and CoA biosynthesis (Fig. 8).

Discussion

Structural modifications of biochar surface characteristics induced by iron modification

FTIR analysis confirmed C-C bonds in both FeBC and BC, with FeBC showing a characteristic Fe-O vibration at 575 cm^{-1}, indicating the presence of Fe-O bonds and confirming the successful loading of iron onto the surface of BC [54]. EDS/XRD verified iron trioxide (Fe_2O_3) deposition on FeBC surfaces, exhibiting uniform C-O-Fe distribution (99.99% purity) with optimal elemental ratios [55]. SEM revealed FeBC's enhanced surface roughness and tubular porosity (Fig. 1), attributed to gas-induced structural dispersion during modification. These modifications increased surface area for improved adsorption performance through enhanced metal complexation, ion exchange capacity, and physical adsorption sites. The permanent iron-carbon bonding via pyrolysis was consistent with previous reports [56, 57].

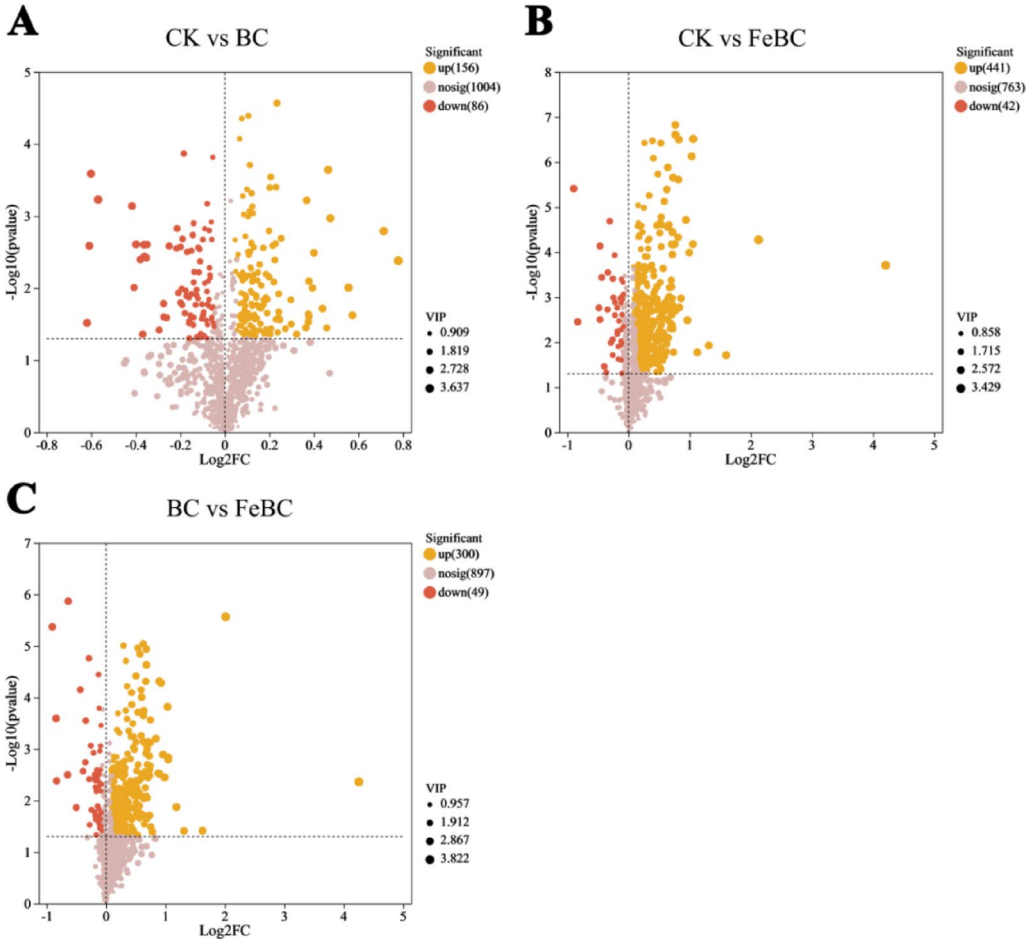

Fig. 6 Comparative metabolomics using volcano plots demonstrating differential root metabolites between (**A**) CK and BC, (**B**) CK and FeBC, and (**C**) BC and FeBC treatment groups

Dual effects of FeBC/BC amendments: enhanced root biomass production coupled with the decrease of Sb accumulation

The addition of both BC and FeBC significantly decreased Sb accumulation in rice roots while promoting plant growth (Fig. 4). The porous structure and high surface area of BC improved water/nutrient retention, sustaining plant nutrition under stress [58, 59]. These findings align with reported BC-induced stress tolerance across plant species, including upregulated gdh3/gdh2 expression in cotton roots that enhances nitrogen assimilation [60]. FeBC demonstrated superior efficacy to BC, potentially through iron film formation on roots that inhibits heavy metal translocation [61]. Although iron plaque formation was not directly examined here, established mechanisms suggest Fe(II) oxidation generates Fe(III)-(oxyhydr)oxide precipitates that restrict metal uptake via surface complexation [62]. Our data indicate FeBC may mimic natural iron plaque function, though controlled rhizosphere studies are needed to verify this mechanism.

Additionally, the application of modified biochar demonstrates enhanced Sb immobilization capacity in environmental systems [23, 26]. Comparative studies reveal that iron-modified rice husk biochar significantly improve Sb immobilization in soil systems, with iron-modified rice husk biochar reducing Pb and Sb bioavailability by 25% and 40% respectively [23]. The 4nZVI-BC (nano-zero-valent iron) variant exhibited particularly high Sb(III) adsorption capacity (93.60 $mg{\cdot}g^{-1}$), representing a 208.6% increase over unmodified biochar [26]. These modifications limit Sb rhizosphere mobility through: Surface complexation, Redox-mediated immobilization. The observed reduction in Sb translocation to rice roots aligns with established mechanisms of metal immobilization by iron-rich amendments [23, 26].

Differential metabolites and associated pathways changed by FeBC

Comparative metabolomic analysis revealed distinct metabolic reprogramming induced by FeBC versus BC (Table 1). Compared to BC, FeBC treatment significantly

Table 1 Differential accumulation patterns of root metabolites in response to biochar and iron-biochar amendments

Class	Metabolite	BC	FeBC	CK
Glycosides	Isowertin 2″-rhamnoside	6.647 ± 0.07860 b	4.393 ± 0.23760 c	7.223 ± 0.05480 a
	Cyanidin 3-O-(6″-malonyl-3″-glucosyl-glucoside)	5.671 ± 0.10260 a	3.922 ± 0.04409 b	5.649 ± 0.01747 a
	2-Hydroxybenzaldehyde O-[xylosyl-(1->6)-glucoside]	4.638 ± 0.16960 b	4.420 ± 0.04409 c	5.133 ± 0.03530 a
	Protocatechuic acid 4-glucoside	4.351 ± 0.82610 a	3.566 ± 0.00926 b	4.677 ± 0.02820 a
	Swertiamarin	4.232 ± 0.56900 a	3.641 ± 0.04409 b	5.076 ± 0.03863 a
	Lepidimoic acid	4.847 ± 0.42500 a	3.727 ± 0.04409 b	5.581 ± 0.09798 a
Organic acid	Lucuminic acid	6.011 ± 0.16210 a	5.680 ± 0.03246 b	6.331 ± 0.02284 a
	Ferulic Acid	5.554 ± 0.40510 a	4.172 ± 0.01716 b	5.527 ± 0.04176 a
	3,4-Dimethoxycinnamic Acid	5.620 ± 0.02495 a	4.593 ± 0.05880 c	5.110 ± 0.16390 b
	Nafenopin	4.445 ± 0.11970 b	3.306 ± 0.00926 c	5.099 ± 0.08874 a
	5-p-Coumaroylquinic acid	4.823 ± 0.24130 a	4.578 ± 0.04410 b	5.368 ± 0.05190 a
	4-Hydroxybutyric acid	4.929 ± 0.06038 a	3.863 ± 0.08534 c	4.472 ± 0.07681 b
Lipids	Osmanthuside A	5.332 ± 0.17800 b	3.359 ± 0.04408 c	5.941 ± 0.05161 a
	Silibinin	6.958 ± 0.19410 b	4.349 ± 0.05379 c	7.395 ± 0.05279 a
	2-Keto-6-acetamidocaproate	5.212 ± 0.02381 b	6.373 ± 0.07964 a	5.147 ± 0.04536 c
	2-Chloromaleylacetate	5.264 ± 0.23850 b	3.398 ± 0.03967 c	5.627 ± 0.08651 a
Coumarin dyes derivatives	Sojagol	5.130 ± 0.32840 b	3.328 ± 0.04408 c	5.850 ± 0.10140 a
	P-Coumaroylagmatine	5.025 ± 0.16490 b	1.247 ± 0.04157 c	5.443 ± 0.39650 a
native compound	Pelargonidin 3-sophoroside	4.358 ± 0.74960 b	3.181 ± 0.04407 c	5.403 ± 0.02001 a
	2,2′-Anhydrocytidine	5.190 ± 0.32550 a	2.537 ± 0.04397 b	5.192 ± 0.07429 a
Alcohols	Galloyl glucose	4.894 ± 0.55150 a	4.373 ± 0.00927 b	5.235 ± 0.02174 a
	Pantetheine	4.812 ± 0.04338 a	3.823 ± 0.05862 b	5.532 ± 0.10590 a
Aldehyde	Sinapoyl aldehyde	5.244 ± 0.12610 a	4.637 ± 0.04383 b	5.512 ± 0.03328 a
	Indole-3-acetaldehyde	5.137 ± 0.04982 a	5.715 ± 0.15630 b	6.041 ± 0.05252 a
Hormones	Luteone	5.324 ± 0.22360 b	2.866 ± 0.04404 c	5.961 ± 0.06758 a
Alkaloids	(S)-Actinidine	2.416 ± 0.03151 c	4.532 ± 0.10180 a	2.432 ± 0.01717 b
Amino acid	Asp-Glu	5.798 ± 0.02869 a	5.563 ± 0.08457 b	6.238 ± 0.02643 a
Alcohols	Pheophorbide a	3.910 ± 0.03163 c	6.084 ± 0.07582 a	5.745 ± 0.68630 b
Acridone derivatives	Acrimarine H	4.210 ± 0.66640 b	3.472 ± 0.04321 c	5.417 ± 0.05871 a
Iminazole derivatives	4-Methylimidazole	4.245 ± 0.08951 a	5.742 ± 0.12360 a	4.152 ± 0.10720 b

reduced the relative abundance of lepidimoic acid, p-coumaroylagmatine, osmanthuside A, silibinin, and sojagol, by 23%, 75%, 37%, 37%, and 35%, respectively. Notably, lepidimoic acid is a stimulating allelopathic substance that can affect various plant hormones and cause plant growth disorders [63]. The suppression of lepidimoic acid suggests a protective mechanism against Sb stress. Concurrently, FeBC enhanced production of defense-related metabolites including indole-3-acetaldehyde, (S)-Actinidine, and phaeophorbide a, by 111%, 187%, and 156%, respectively (Table 1). These changes correlate with activated indole-based pathogen defense pathways [64] and alkaloid-mediated growth regulation [65].

The observed increases in traumatic, shikimic and citric acids further indicate the role of FeBC in stress-responsive metabolic restructuring. Correlation analyses revealed functional connections between FeBC-induced metabolic changes, root development and Sb accumulation (Fig. S1). For example, FeBC increased the exudation of traumatic acid, which was associated with enhanced root growth, consistent with its established growth-promoting function [66]. Shikimic acid participates in flavonoid biosynthesis and reactive oxygen species scavenging [67, 68]. The accumulation of shikimic acid induced by FeBC indicates an enhanced antioxidant capacity of rice under Sb stress. Furthermore, FeBC increased the content of citric acid, which may chelate HMs and alter their mobility [69]. The elevated citric acid content induced by FeBC suggests that addition of the amendment material increased the dual protective mechanisms of the plant including (1) modulating enzymatic activities and metabolic processes to improve stress tolerance, and (2) reducing Sb translocation through metal complexation. Taken together, these findings demonstrate that the addition of FeBC mediates rice responses to Sb stress through metabolic reprogramming, which directly influencing HM translocation capacity and stress defence mechanisms via coordinated changes in root metabolite profiles.

In addition, FeBC mainly impacted five metabolic pathways including (1) phenylalanine, tyrosine and tryptophan biosynthesis, (2) phenylpropanoid biosynthesis, (3) lysine degradation, (4) tryptophan metabolism, and (5) pantothenate and CoA biosynthesis (Fig.

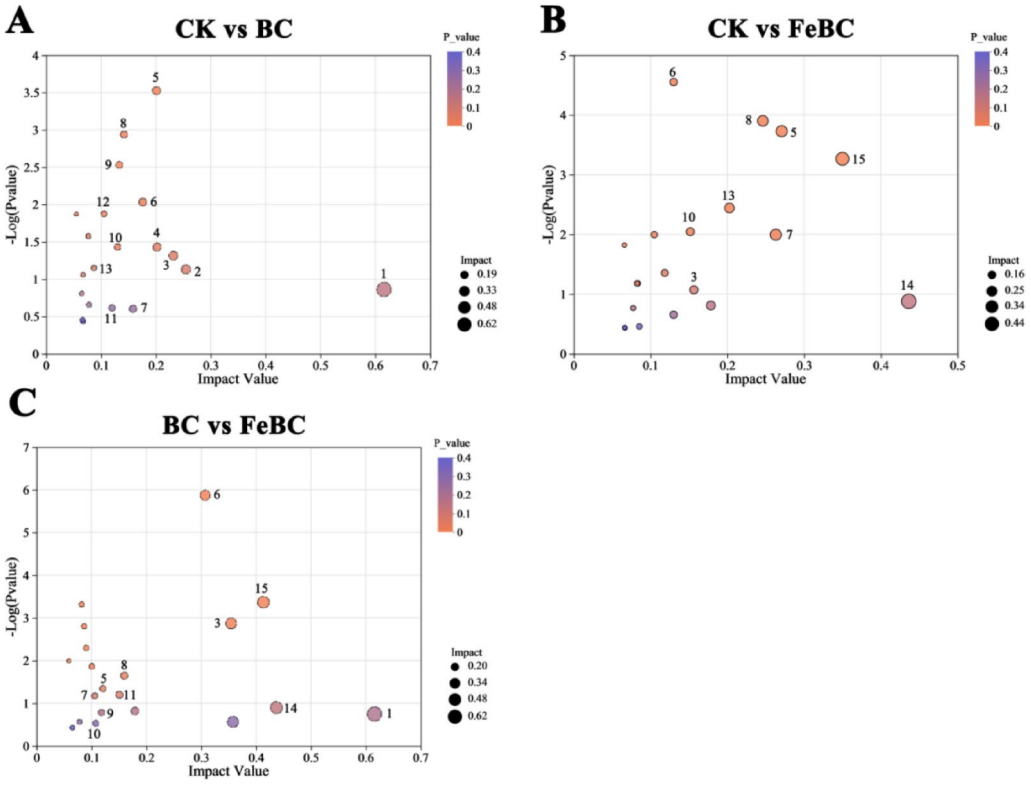

Fig. 7 KEGG pathway analysis of root metabolites showing differential regulation between **A** CK and BC, **B** CK and FeBC, and **C** BC and FeBC treatment groups. (1) betalain biosynthesis, (2) starch and sucrose metabolism, (3) pantothenate and CoA biosynthesis, (4) biotin metabolism, (5) lysine degradation, (6) phenylalanine, tyrosine and tryptophan biosynthesis, (7) tropane, piperidine and pyridine metabolism, (8) phenylpropanoid biosynthesis, (9) galactose metabolism, (10) valine, leucine and isoleucine biosynthesis, (11) arginine biosynthesis, (12) arginine and proline metabolism, (13) lysine biosynthesis, (14) arachidonic acid metabolism, (15) tryptophan metabolism

8). Phenylalanine, tyrosine and tryptophan are primarily used in protein synthesis and serve as precursors for many natural plant products, including cell wall components, pigments and hormones [70]. These amino acids enable plant cell walls to harden, thereby reducing their exposure to biological and non-biological environmental stresses [71]. For example, Cd stress impacts the biosynthesis of these amino acids, enhancing the antioxidant capacity of plants, promoting growth, and strengthening defence responses [72]. This study demonstrated that applying FeBC resulted in the up-regulation of these amino acid synthesis pathways in plants, helping rice resist Sb stress.

The phenylpropanoid biosynthetic pathway produces and accumulates various phenolic compounds that inhibit the production of harmful reactive oxygen species. This pathway can be activated in response to abiotic stresses, such as HMs and drought [73]. It has been demonstrated that rice can mitigate the environmental impact of Cd through phenylpropanoid biosynthesis [74]. This study showed that adding a FeBC can stimulate these synthetic pathways, potentially acting as a signalling molecule to help plants respond to Sb stress.

Lysine is an essential amino acid for plant growth and development. It is also involved in transcriptional and post-transcriptional control in individual plants [75]. Enhancing the lysine degradation pathway increases the activity of antioxidant enzymes in plants, thereby reducing Cd stress and improving yield and quality [76]. This study demonstrated that adding a FeBC increased the activity of the lysine degradation pathway, thereby enhancing rice tolerance to Sb stress.

Pantothenate and CoA can enhance plant nutrition and growth, thereby boosting their resilience to adverse environmental conditions. For example, the biosynthesis pathways of pantothenate and coenzymes are enriched in salt-stressed Zygophyllum plants [77]. CoA plays a crucial role in the storage and accumulation of lipids [78]. It has been shown that maize roots promote their own growth by synthesising pantothenate and CoA, thereby reducing their absorption of Cd [79]. This study indicates that adding FeBC significantly stimulates the biosynthesis of pantothenate and CoA in rice, helping the plant to regulate its defence mechanism and resist Sb stress.

Tryptophan metabolism is an important component of the plant immune system [80]. When plants experience environmental stress, the tryptophan metabolic pathway

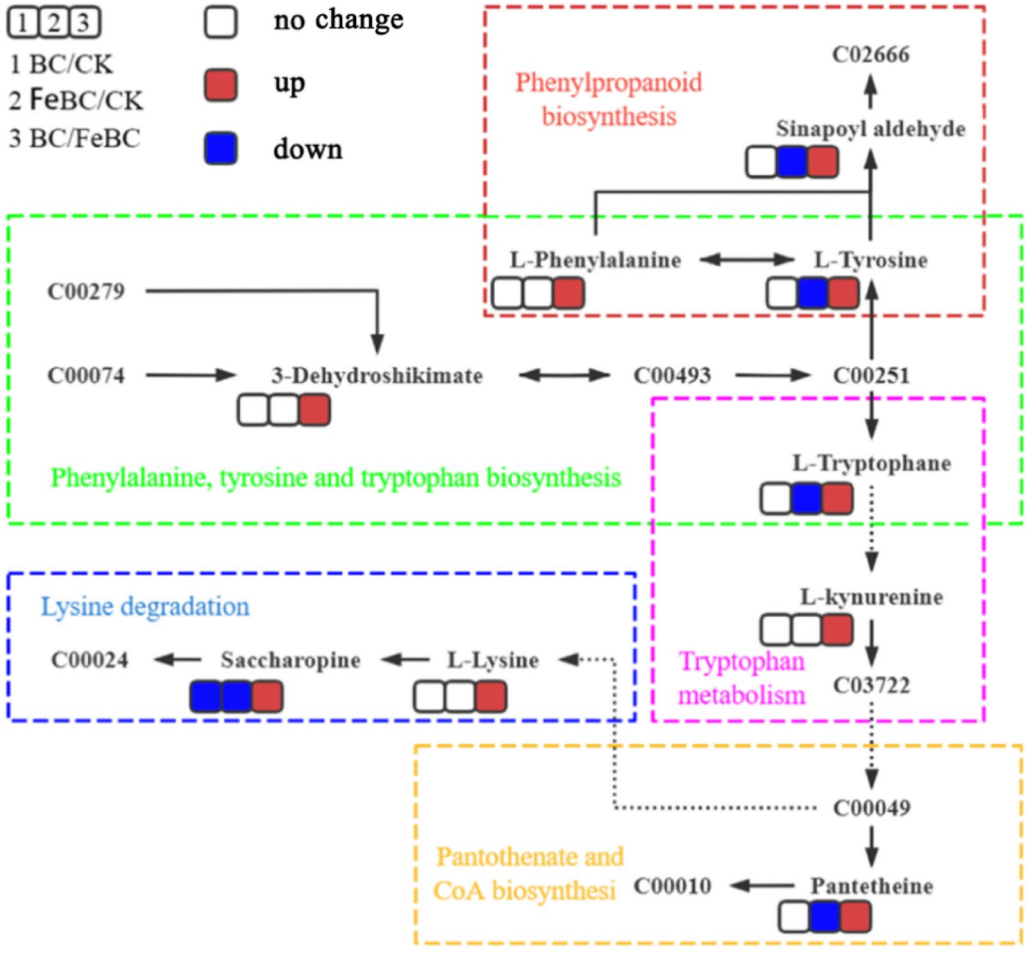

Fig. 8 A comprehensive overview of treatment-induced alterations in root metabolome

acts as a signalling molecule that activates the production of growth-promoting substances [81]. Furthermore, tryptophan metabolism can enhance tolerance to HMs and promote growth by regulating auxins, such as indole-3-acetic acid [82].

Overall, we hypothesise that FeBC mitigates the accumulation of Sb in rice via three integrated mechanisms: (1) Surface modification: Fe-oxide enrichment increases the specific surface area and the number of adsorption sites, thereby enhancing metal complexation and ion exchange capacity. (2) Physical barrier: the hierarchical pore structure facilitates Sb adsorption and induces iron plaque formation, thereby reducing soluble Sb in the rhizosphere. (3) Rhizosphere regulation: FeBC alters root exudation, thereby improving plant tolerance. Together, these mechanisms limit Sb translocation while improving rice growth under Sb stress.

Conclusions

This study elucidates the dual functionality of hydrothermally synthesized FeBC in simultaneously (1) enhancing root biomass and (2) reducing grain Sb accumulation. Metabolomic analyses identified key pathway modulations that concurrently promote stress tolerance and growth vigor. The technique is applicable to Sb-contaminated rice fields and has the potential to improve food security without compromising yields. Limitations of the technique include uncharacterized Sb speciation, undefined recovery rates, and incomplete material characterization (surface area/porosity). Field applicability may vary with soil properties (pH, organic matter) and crop genotypes. Future work should employ X-ray absorption near-edge structure and column leaching tests to evaluate practical feasibility. Nevertheless, these findings advance biochar-based solutions for simultaneous soil remediation and agricultural productivity in developing regions.

Abbreviations

SEM	Scanning electron microscopy
EDS	Energy dispersive spectrometer
XRD	X-ray diffraction
HM	Heavy metal
PPF	Pomelo peel flesh
Sb	Antimony
BC	Pristine biochar

FeBC	Iron-modified biochar
As	Arsenic
Cd	Cadmium
Pb	Lead
Zn	Zinc
Cr	Chromium

Supplementary Information

The online version contains supplementary material available at https://doi.org/10.1186/s12870-025-07071-y.

Supplementary Material 1

Acknowledgements
Not applicable.

Author contributions
R.D. and F.M wrote the main manuscript text, form analysis, fund acquisition and verification. H.Y and Q.D have prepared Figs. 1, 2, 3, 4, 5, 6, 7 and 8. Y.Z and Y.D have carried out experimental research and investigation. All the authors have reviewed the manuscript.

Funding
This work was supported by grants from the National Natural Science Foundation of China (32371589), Natural Science Foundation of Hunan Province (2024JJ7238, 2023JJ50475), and the Aid program for Science and Technology Innovative Research Team in Higher Educational Institutions of Hunan Province (201937924).

Data availability
The datasets analyzed during the current study are available from the corresponding author on reasonable request.

Declarations

Ethics approval and consent to participate
Rice seedlings were collected from the Loudi Agricultural Science Institute in Hunan and identified by Professor Duan Renyan. The methods involved in this study were conducted in accordance with local and national regulations.

Consent for publication
All the authors agreed to publish.

Competing interests
The authors declare no competing interests.

Author details
[1]College of Agriculture and Biotechnology, Hunan University of Humanities, Science and Technology, Loudi 417000, Hunan, China
[2]Key Laboratory of Development, Utilization, Quality and Safety Control of Characteristic Agricultural Resources in Central Hunan Province, Loudi 417000, Hunan, China

Received: 26 December 2024 / Accepted: 15 July 2025
Published online: 08 August 2025

References

1. Zhu Y, Yang J, Wang L, Lin Z, Dai J, Wang R, et al. Factors influencing the uptake and speciation transformation of antimony in the soil-plant system, and the redistribution and toxicity of antimony in plants. Sci Total Environ. 2020;738: 140232.
2. Bolan N, Kumar M, Sing E, Kumar A, Singh L, Kumar S, et al. Antimony contamination and its risk management in complex environmental settings: A review. Environ Int. 2022;158:106908.
3. Fan J, Chen Y, Li X, Huang J, Zhang X, Chen K, et al. Transcriptomic and metabolomic insights into the antimony stress response of tall fescue (*Festuca arundinacea*). Sci Total Environ. 2024;933: 172990.
4. Zhao Q, Li J, Tan Z, Li W, Zhang Z, Guan X. Collaborative effects of antimony-arsenic contaminations on microbial communities in the typical antimony mining areas of Southwest China. Sci Total Environ. 2025;975: 179249.
5. Tang H, Meng G, Xiang J, Mahmood A, Xiang G, Liu Y, et al. Toxic effects of antimony in plants: reasons and remediation possibilities—a review and future prospects. Front Plant Sci. 2022;13:1011945.
6. Ran M, Wu J, Jiao Y, Li J. Biosynthetic selenium nanoparticles (Bio-SeNPs) mitigate the toxicity of antimony (Sb) in rice (*Oryza sativa* L.) by limiting Sb uptake, improving antioxidant defense system and regulating stress-related gene expression. J Hazard Mater. 2024;470: 134263.
7. Haider FU, Zulfiqar U, Ain NU, Mehmood T, Ali U, Ramos Aguila LC, et al. Managing antimony pollution: insights into soil–plant system dynamics and remediation strategies. Chemosphere. 2024;362: 142694.
8. Wang X, Li F, Yuan C, Li B, Liu T, Liu C, et al. The translocation of antimony in soil-rice system with comparisons to arsenic: alleviation of their accumulation in rice by simultaneous use of Fe (II) and NO_3^-. Sci Total Environ. 2019;650:633–41.
9. Feng R, Lei L, Su J, Zhang R, Zhu Y, Chen W, et al. Toxicity of different forms of antimony to rice plant: effects on root exudates, cell wall components, endogenous hormones and antioxidant system. Sci Total Environ. 2020;711: 134589.
10. Lai Z, He M, Lin C, Ouyang W, Liu X. Interactions of antimony with biomolecules and its effects on human health. Ecotoxicol Environ Saf. 2022;233: 113317.
11. Wu TL, Cui XD, Cui PX, Ata-Ul-Karim ST, Sun Q, Liu C, et al. Speciation and location of arsenic and antimony in rice samples around antimony mining area. Environ Pollut. 2019;252:1439–47.
12. Yaashikaa PR, Kumar PS, Jeevanantham S, Saravanan. RA. review on bioremediation approach for heavy metal detoxification and accumulation in plants. Environ Pollut. 2022;301:119035.
13. Kalina M, Sovova S, Svec J, Trudicova M, Hajzler J, Kubikova L, et al. The effect of pyrolysis temperature and the source biomass on the properties of biochar produced for the agronomical applications as the soil conditioner. Materials. 2022;15(24):8855.
14. Nguyen TB, Sherpa K, Bui XT, Nguyen VT, Vo TD, Ho HT, et al. Biochar for soil remediation: a comprehensive review of current research on pollutant removal. Environ Pollut. 2023;337: 122571.
15. Tang H, Hassan MU, Nawaz M, Yang W, Liu Y, Yang B. A review on sources of soil antimony pollution and recent progress on remediation of antimony polluted soils. Ecotox Environ Safe. 2023;266:115583.
16. Kottis T, Soursos N, Govatsi K, Sygellou L, Vakros J, Manariotis ID, et al. Biochar from Olive tree twigs and spent malt rootlets as electrodes in Zn-air batteries. J Colloid Interf Sci. 2024;665:10–8.
17. Yu Z, Qiu W, Wang F, Lei M, Wang D, Song Z. Effects of manganese oxide-modified biochar composites on arsenic speciation and accumulation in an *Oryza sativa* L. cultivar. Chemosphere. 2017;168:341–9.
18. Li J, Gao Y, Li C, Wang F, Chen H, Yang X, et al. Pristine and Fe-functionalized biochar for the simultaneous immobilization of arsenic and antimony in a contaminated mining soil. J Hazard Mater. 2024;469: 133937.
19. Guo J, Yan C, Luo Z, Fang H, Hu S, Cao Y. Synthesis of a novel ternary HA/Fe-Mn oxides-loaded Biochar composite and its application in cadmium (II) and arsenic (V) adsorption. J Environ Sci. 2019;85:168–76.
20. Yang H, Ye C, Wang J, Jin H, Zhang J, Wang X, et al. Mechanism study of toluene removal using iron/nickel bimetallic catalysts supported on biochar. Sci Total Environ. 2024;925: 171732.
21. Algethami JS, Irshad MK, Javed W, Alhamami MAM, Ibrahim M. Iron-modified biochar improves plant physiology, soil nutritional status and mitigates Pb and Cd-hazard in wheat (*Triticum aestivum* L). Front Plant Sci. 2023;14:1221434.
22. Li X, Li R, Zhan M, Hou Q, Zhang H, Wu G, et al. Combined magnetic biochar and ryegrass enhanced the remediation effect of soils contaminated with multiple heavy metals. Environ Int. 2024;185: 108498.
23. Teng F, Zhang Y, Wang D, Shen M, Hu D. Iron-modified rice husk hydrochar and its immobilization effect for Pb and Sb in contaminated soil. J Hazard Mater. 2020;398:122977.
24. Tang H, Meng G, Jiang W, Ma Y, Duan R, Hassan MU, et al. Co-application of iron modified Biochar and metal resistant bacteria alleviates antimony toxicity in rice by modulating morpho-physiological and biochemical traits and soil microbial activities. Environ Technol Inno. 2025;38:104184.

25. Samsuri AW, Sadegh-Zadeh F, Seh-Bardan BJ. Adsorption of As(III) and As(V) by Fe coated biochars and biochars produced from empty fruit bunch and rice husk. J Environ Chem Eng. 2013;1:981–8.
26. Ma S, Ji J, Mou Y, Shen X, Xu S. Enhanced adsorption for trivalent antimony by nano-zero-valent iron-loaded biochar: performance, mechanism, and sustainability. Environ SCI Pollut R. 2023;30(52):112536–47.
27. Vives-Peris V, de Ollas C, Gómez-Cadenas A, Pérez-Clemente RM. Root exudates: from plant to rhizosphere and beyond. Plant Cell Rep. 2020;39(1):3–17.
28. Sun L, Cao X, Tan C, Deng Y, Cai R, Peng X, et al. Analysis of the effect of cadmium stress on root exudates of Sedum Plumbizincicola based on metabolomics. Ecotox Environ Safe. 2020;205:111152.
29. Liu X, Wan Y, Liu P, Fu Y, Zou W. A novel activated carbon prepared from grapefruit peel and its application in removal of phenolic compounds. Water Sci Technol. 2018;77(9–10):2517–27.
30. Yu H, Gu L, Chen L, Wen H, Zhang D, Tao H. Activation of grapefruit derived biochar by its peel extracts and its performance for tetracycline removal. Bioresource Technol. 2020;316:123971.
31. Nowicki P, Kazmierczak-Razna J, Pietrzak R. Physicochemical and adsorption properties of carbonaceous sorbents prepared by activation of tropical fruit skins with potassium carbonate. Mater Des. 2016;90:579–85.
32. Zhang C, Pan R, Wang H, Liu Y, Bai R, Zhang H, et al. Pomelo Peel biomass derived highly active advanced-oxidation-process catalyst: complete elimination of organic pollutants. J Colloid Interf Sci. 2024;670:50–60.
33. Wang J, Zhang M. Adsorption characteristics and mechanism of bisphenol a by magnetic Biochar. Int J Env Res Pub He. 2020;17(3):1075.
34. Lyu H, Tang J, Cui M, Gao B, Shen B. Biochar/iron (BC/Fe) composites for soil and groundwater remediation: synthesis, applications, and mechanisms. Chemosphere. 2020;246:125609.
35. Jung KW, Lee SY, Lee YJ. Facile one-pot hydrothermal synthesis of cubic spinel-type manganese ferrite/biochar composites for environmental remediation of heavy metals from aqueous solutions. Bioresource Ttchnol. 2018;261:1–9.
36. Masuku M, Nure JF, Atagana HI, Hlongwa N, Nkambule TTI. Pinecone biochar for the adsorption of chromium (VI) from wastewater: kinetics, thermodynamics, and adsorbent regeneration. Environ Res. 2024;258: 119423.
37. Wang L, Gao C, Yang K, Sheng Y, Xu J, Zhao Y, et al. Effects of biochar aging in the soil on its mechanical property and performance for soil CO_2 and N_2O emissions. Sci Total Environ. 2021;782: 146824.
38. Abdu M, Babaee S, Worku A, Msagati TAM, Nure JF. The development of giant reed biochar for adsorption of basic blue 41 and eriochrome black T. azo dyes from wastewater. Sci Rep. 2024;14(1):18320.
39. Alghamdi AG, Alasmary Z. Efficient remediation of cadmium- and lead-contaminated water by using Fe-modified date palm waste biochar-based adsorbents. Int J Env Res Pub He. 2023;20(1):802.
40. Manawi Y, Al-Gaashani R, Simson S, Tong Y, Lawler J, Kochkodan V. Adsorptive removal of phosphate from water with biochar from acacia tree modified with iron and magnesium oxides. Sci Rep. 2024;14(1):17414.
41. Yang X, Wen E, Ge C, El-Naggar A, Yu H, Wang S, et al. Iron-modified phosphorus- and silicon-based biochars exhibited various influences on arsenic, cadmium, and lead accumulation in rice and enzyme activities in a paddy soil. J Hazard Mater. 2023;443: 130203.
42. Babatunde EO, Gurav R, Hwang SS. Pistia stratiotes L. Biochar for sorptive removal of aqueous inorganic nitrogen materials. Materials. 2024;17(15):3858.
43. Xu B, Wang F, Zhang Q, Lan Q, Liu C, Guo X, et al. Influence of iron plaque on the uptake and accumulation of chromium by rice (*Oryza sativa* L.) seedlings: insights from hydroponic and soil cultivation. Ecotox Environ Safe. 2018;162:51–8.
44. Zhou X, Sun C, Zhu P, Liu F. Effects of antimony stress on photosynthesis and growth of *Acorus calamus*. Front Plant Sci. 2018;9:579.
45. Sheng L, Hao C, Guan S, Huang Z. Spatial distribution, geochemical behaviors and risk assessment of antimony in rivers around the antimony mine of xikuangshan, Hunan province, China. Water Sci Technol. 2022;85(4):1141–54.
46. Duan R, Lin Y, Yang L, Zhang Y, Hu W, Du Y, et al. Effects of antimony stress on growth, structure, enzyme activity and metabolism of Nipponbare rice (*Oryza sativa* L.) roots. Ecotox Environ Safe. 2023;249:114409.
47. Jia W, Ma C, White JC, Yin M, Cao H, Wang J, et al. Effects of biochar on 2, 2′, 4, 4′, 5, 5′-hexabrominated diphenyl ether (BDE-153) fate in *Amaranthus mangostanus* L.: accumulation, metabolite formation, and physiological response. Sci Total Environ. 2019;651:1154–65.
48. Aali N, Alemzadeh Ansari N, Zahedi SM. Development of sustainable strawberry production in closed cultivation systems: effects of bagasse biochar on morphological and physiological attributes, yield and autotoxic changes. J Environ Manage. 2024;371: 123100.
49. Chen Z, Tang YT, Zhou C, Xie ST, Xiao S, Baker AJM, et al. Mechanisms of Fe biofortification and mitigation of cd accumulation in rice (*Oryza sativa* L.) grown hydroponically with Fe chelate fertilization. Chemosphere. 2017;175:275–85.
50. Pan D, Liu C, Yu H, Li F. A paddy field study of arsenic and cadmium pollution control by using iron-modified Biochar and silica Sol together. Environ Sci Pollut R. 2019;26(24):24979–87.
51. Yang X, Wang C, Huang Y, Liu B, Liu Z, Huang Y, et al. Foliar application of the sulfhydryl compound 2,3-dimercaptosuccinic acid inhibits cadmium, lead, and arsenic accumulation in rice grains by promoting heavy metal immobilization in flag leaves. Environ Pollut. 2021;285: 117355.
52. Desalew A, Mehari B. Variations in elemental composition of rice (*Oryza sativa* L.) with different cultivation areas of Ethiopia. PLoS One. 2023;18(10):e0290073.
53. Wright EJ, Beach DG, McCarron P. Non-target analysis and stability assessment of reference materials using liquid chromatography–high-resolution mass spectrometry. Anal Chim Acta. 2022;1201: 339622.
54. Xin O, Yitong H, Xi C, Jiawei C. Magnetic biochar combining adsorption and separation recycle for removal of chromium in aqueous solution. Water Sci Technol. 2017;75(5–6):1177–84.
55. Ahmed Khan B, Ahmad M, Bolan N, Farooqi A, Iqbal S, Mickan B, et al. A mechanistic approach to arsenic adsorption and immobilization in aqueous solution, groundwater, and contaminated paddy soil using pine-cone magnetic Biochar. Environ Res. 2024;245:117922.
56. Silva TCF, VergÜtz L, Pacheco AA, Melo LF, Renato NS, Melo LCA. Characterization and application of magnetic Biochar for the removal of phosphorus from water. Acad Bras Cienc. 2020;92(3):e20190440.
57. Li X, Liu W, Zhang J, Wang Z, Guo Z, Ali J, et al. Effective removal of microplastics by filamentous algae and its magnetic biochar: performance and mechanism. Chemosphere. 2024;358:142152.
58. Khan Z, Zhang K, Khan MN, Bi J, Zhu K, Luo L, et al. How biochar affects nitrogen assimilation and dynamics by interacting soil and plant enzymatic activities: quantitative assessment of 2 years potted study in a rapeseed-soil system. Front Plant Sci. 2022;13:853449.
59. Zhang K, Han X, Fu Y, Zhou Y, Khan Z, Bi J, et al. Biochar coating as a cost-effective delivery approach to promoting seed quality, rice germination, and seedling establishment. Plants. 2023;12(22):3896.
60. Feng L, Xu W, Tang G, Gu M, Geng Z. Biochar induced improvement in root system architecture enhances nutrient assimilation by cotton plant seedlings. BMC Plant Biol. 2021;21(1):269.
61. Chen G, Taherymoosavi S, Cheong S, Yin Y, Akter R, Marjo CE, et al. Advanced characterization of biomineralization at plaque layer and inside rice roots amended with iron- and silica-enhanced biochar. Sci Rep. 2021;11(1):159.
62. Irshad MK, Zhu S, Javed W, Lee JC, Mahmood A, Lee SS, et al. Risk assessment of toxic and hazardous metals in paddy agroecosystem by biochar-for biomembrane applications. Chemosphere. 2023;340:139719.
63. Yamada K, Hondo M, Shigemori H, Hirose K, Hasegawa K. Physiological effects of lepidimoic acid (a stimulatory allelochemical) on cucumber cotyledons. Allelopathy J. 2010;25(2):497–502.
64. Böttcher C, Chapman A, Fellermeier F, Choudhary M, Scheel D, Glawischnig E. The biosynthetic pathway of indole-3-carbaldehyde and indole-3-carboxylic acid derivatives in *Arabidopsis*. Plant Physiol. 2014;165(2):841–53.
65. Bhambhani S, Kondhare KR, Giri AP. Diversity in chemical structures and biological properties of plant alkaloids. Molecules. 2021;26(11):3374.
66. Wu ZZ, Gan ZW, Zhang YX, Chen SB, Gan CD, Yang K, et al. Transcriptomic and metabolomic perspectives for the growth of alfalfa (*Medicago sativa* L.) seedlings with the effect of vanadium exposure. Chemosphere. 2023;336:139222.
67. Wang R, Lin K, Chen H, Qi Z, Liu B, Cao F, et al. Metabolome analysis revealed the mechanism of exogenous glutathione to alleviate cadmium stress in maize (*Zea mays* L.) seedlings. Plants. 2021;10(1):105.
68. Ling Y, Tan M, Xi Y, Li Z. Differential drought tolerance among dichondra (*Dichondra repens*) genotypes in relation to alterations in chlorophyll metabolism, osmotic adjustment, and accumulation of organic metabolites. Protoplasma. 2024;261(5):897–909.
69. Khatun MR, Mukta RH, Islam MA, Huda AKMN. Insight into citric acid-induced chromium detoxification in rice (*Oryza sativa* L). Int J Phytoremediat. 2019;21(12):1234–40.
70. Parthasarathy A, Cross PJ, Dobson RCJ, Adams LE, Savka MA, Hudson AO. A three-ring circus: metabolism of the three proteogenic aromatic amino acids and their role in the health of plants and animals. Front Mol Biosci. 2018;5: 29.

71. El-Azaz J, Moore B, Takeda-Kimura Y, Yokoyama R, Wijesingha Ahchige M, Chen X, et al. Coordinated regulation of the entry and exit steps of aromatic amino acid biosynthesis supports the dual lignin pathway in grasses. Nat Commun. 2023;14(1):7242.
72. Zemanová V, Pavlík M, Pavlíková D. Cadmium toxicity induced contrasting patterns of concentrations of free sarcosine, specific amino acids and selected microelements in two *Noccaea* species. PLoS One. 2017;12(5):e0177963.
73. Sharma A, Shahzad B, Rehman A, Bhardwaj R, Landi M, Zheng B. Response of phenylpropanoid pathway and the role of polyphenols in plants under abiotic stress. Molecules. 2019;24(13):2452.
74. Liu J, Lv Y, Li M, Wu Y, Li B, Wang C, et al. Peroxidase in plant defense: novel insights for cadmium accumulation in rice (*Oryza sativa* L). J Hazard Mater. 2024;474: 134826.
75. Kishor PBK, Suravajhala R, Rajasheker G, Marka N, Shridhar KK, Dhulala D, et al. Lysine, lysine-rich, serine, and serine-rich proteins: link between metabolism, development, and abiotic stress tolerance and the role of Ncrnas in their regulation. Front Plant Sci. 2020;11:546213.
76. An M, Chang D, Wang X, Wang K. Protective effects of polymer amendment on specific metabolites in soil and cotton leaves under cadmium contamination. Ecotoxicol Environ Saf. 2023;264: 115463.
77. Wang J, Jiang X, Zhao C, Fang Z, Jiao P. Transcriptomic and metabolomic analysis reveals the role of coa in the salt tolerance of *Zygophyllum* spp. BMC Plant Biol. 2020;20(1):9.
78. Rubio S, Whitehead L, Larson TR, Graham IA, Rodriguez PL. The coenzyme A biosynthetic enzyme phosphopantetheine adenylyltransferase plays a crucial role in plant growth, salt/osmotic stress resistance, and seed lipid storage. Plant Physiol. 2008;148(1):546–56.
79. Zhao M, Li Y, Li C, Wang X, Cao B, Zhang J, et al. Effects of polyurethane microplastics combined with cadmium on maize growth and cadmium accumulation under different long-term fertilisation histories. J Hazard Mater. 2024;473: 134726.
80. Xia S, Ruan B, Rao Y, Cui Y, Zhang Q, Zeng D, et al. The ell1 mutation disrupts Tryptophan metabolism and induces cell death. Plant Signal Behav. 2021;16(6):1905336.
81. Wan D, Wan Y, Zhang T, Wang R, Ding Y. Multi-omics analysis reveals the molecular changes accompanying heavy-grazing-induced dwarfing of *Stipa grandis*. Front Plant Sci. 2022;13:995074.
82. Li Y, Qi X. Tryptophan pretreatment adjusts transcriptome and metabolome profiles to alleviate cadmium toxicity in Arabidopsis. J Hazard Mater. 2023;452: 131226.

Publisher's Note